

Electronic structure and magnetism in infinite-layer nickelates RNiO_2 (R= La-Lu)

Jesse Kapeghian¹ and Antia S. Botana^{1,*}

¹*Department of Physics, Arizona State University, Tempe, AZ - 85287, USA*

(Dated: January 9, 2022)

Using first-principles calculations, we analyze the evolution of the electronic structure and magnetic properties of infinite-layer nickelates RNiO_2 (R= rare-earth) as R changes across the lanthanide series from La to Lu. By correlating these changes with in-plane and out-of-plane lattice parameter reductions, we conclude that the in-plane Ni-O distance is the relevant control parameter in infinite-layer nickelates. An antiferromagnetic ground state is obtained for all RNiO_2 (R=La-Lu). This antiferromagnetic state remains metallic across the lanthanide series and is defined by a multi-orbital picture with low-energy relevance of a flat Ni- d_{z^2} band pinned at the Fermi level, in contrast to cuprates. Other non-cuprate-like properties such as the involvement of R- d bands at the Fermi level and a large charge transfer energy are robust for all RNiO_2 materials.

I. INTRODUCTION

The collection of characteristics sought for when looking for cuprate analogs include a layered structure, proximity to a d^9 ($S=1/2$) configuration analog to Cu^{2+} , $d_{x^2-y^2}$ states as the active orbitals, antiferromagnetic correlations, and strong p-d hybridization¹. Perovskite RNiO_3 -based heterostructures (R = rare-earth) have been intensively studied over the last decade motivated by predictions of superconductivity based on their analogies to cuprates²⁻⁶. A plethora of new phenomena have been discovered in these systems, due to the interplay of epitaxial strain, quantum confinement, and interfacial effects. However, the promise of RNiO_3 -based heterostructures for superconductivity is yet to be realized^{4,6}.

In this regard, one alternative to heterostructures based on perovskite phases are low-valence layered nickelates $\text{R}_{n+1}\text{Ni}_n\text{O}_{2n+2}$ ($n= 2, 3... \infty$), closer to cuprates in terms of their structure (with infinite NiO_2 planes) as well as in terms of electron count (close to d^9)⁷⁻¹⁰. The realization of this promise came with the recent report of the first superconducting nickelate: hole-doped NdNiO_2 ¹¹⁻¹³. RNiO_2 (112) materials are the infinite-layer members of the series and realize the hard to stabilize Ni^{1+} oxidation state, isoelectronic with Cu^{2+} ¹⁴. These materials are derived via oxygen reduction from the corresponding perovskite phase RNiO_3 (113)¹⁵⁻¹⁹. To date, only the Nd and La variants of 112 materials have been realized in bulk form¹⁵⁻¹⁹. However, parent perovskite 113 phases exist for R=Lu-La, and their phase diagram is well established⁵. Except for R = La, all rare-earth perovskite 113 nickelates exhibit a metal-insulator phase transition (MIT), accompanied by a symmetry lowering from orthorhombic to monoclinic^{4,5}. At a temperature lower than T_{MIT} , they undergo an antiferromagnetic (AFM) phase transition. The evolution of these transitions can be correlated with structural changes upon a change in rare-earth. In particular, the Goldschmidt tolerance factor (that serves as a measurement of the tendency of the structure to distort) is often advocated in this regard- a decrease in tolerance factor with R tends to reduce the Ni-O-Ni angle with a subse-

TABLE I. In-plane (a) and out-of-plane (c) ab-initio optimized lattice parameters for RNiO_2 (R= rare-earth) within GGA.

| Rare-earth | a (Å) | c (Å) |
|------------|---------|---------|
| La | 3.960 | 3.370 |
| Pr | 3.940 | 3.341 |
| Nd | 3.926 | 3.302 |
| Pm | 3.912 | 3.263 |
| Sm | 3.902 | 3.237 |
| Eu | 3.890 | 3.206 |
| Gd | 3.879 | 3.177 |
| Tb | 3.869 | 3.155 |
| Dy | 3.861 | 3.133 |
| Ho | 3.856 | 3.110 |
| Er | 3.849 | 3.090 |
| Tm | 3.841 | 3.070 |
| Yb | 3.834 | 3.053 |
| Lu | 3.828 | 3.034 |

quent reduction of the overlap between the Ni- d and O- p orbitals^{5,6}.

Exploiting the prospect that other perovskite nickelate 113 phases could be reduced to their respective 112 counterpart, we analyze here the electronic structure and magnetism of RNiO_2 materials (R= La-Lu). We correlate changes in R with modifications of the in-plane and out-of-plane lattice parameters in LaNiO_2 (the extreme member of the lanthanide series) and analyze the effects of these changes in their electronic and magnetic properties. We conclude that the Ni-O in-plane distance is the control parameter in RNiO_2 nickelates as modifications of the out-of-plane lattice parameter do not give rise to appreciable changes in the electronic structure. We find that all infinite-layer nickelates have an antiferromagnetic ground state from first principles, but this state is fundamentally different from that of cuprates as it is metallic and has Ni- d_{z^2} states as active orbitals (in addition to the naively expected $d_{x^2-y^2}$ ones).

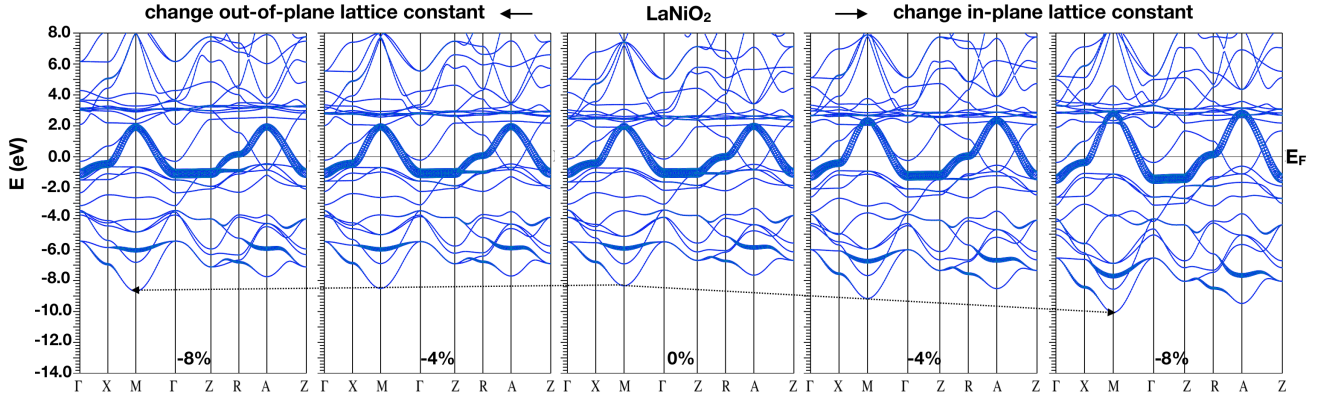


FIG. 1. GGA non-magnetic LaNiO_2 band structure with band character plot ($\text{Ni-d}_{x^2-y^2}$ highlighted) at the experimental lattice constants (0%, central panel), upon reduction of in-plane (right panels) and out-of-plane (left panels) lattice parameters. The arrows are a guide to show the drastic changes in the bandstructure upon an in-plane lattice constant reduction in contrast to the negligible changes upon an out-of-plane lattice constant reduction. Appendix Fig. A2 shows a zoomed-in version of the band structures around the Fermi level.

II. COMPUTATIONAL DETAILS

We performed two separate sets of density functional theory (DFT)-based calculations for RNiO_2 nickelates. 1) *Calculations with a different rare-earth ion.* We performed calculations for 112 compounds across the lanthanide series ($\text{R} = \text{La-Lu}$) using PAW pseudopotentials²⁰ as implemented in the VASP code^{21,22} placing the R-4f electrons in the core. We note that the role of 4f states in NdNiO_2 has been analyzed in the literature in connection to its normal and superconducting state properties²³. It would be worth analyzing what aspects of the electronic structure and magnetic properties of RNiO_2 materials may be affected from the open 4f shell for other R ions but we leave that for future work. 2) *Calculations for LaNiO_2 at different in-plane and out-of-plane lattice constants.* These calculations were performed using the all-electron, full potential code WIEN2k^{24,25} based on the augmented plane wave plus local orbitals (APW + lo) basis set keeping the La-4f states present. As a starting point, the experimental LaNiO_2 lattice constants were used¹⁶ ($a = 3.96 \text{ \AA}$, $c = 3.37 \text{ \AA}$). Using reduced lattice parameters in LaNiO_2 allows us to mimic the effect of a smaller R ion (the size of R decreases with increasing atomic number) and determine if the changes in electronic structure and magnetic properties upon R variation are linked mostly to the explicit R change, or to in-plane (a) and/or out-of-plane (c) lattice constant changes.

The Perdew-Burke-Ernzerhof version of the generalized gradient approximation (GGA)²⁶ was used for both WIEN2k and VASP structural relaxations, and for non-magnetic calculations. In order to properly account for correlation effects in the Ni-d electrons, an on-site Coulomb repulsion U was included in spin-polarized calculations, using the GGA+ U method within the fully localized limit (FLL)²⁷. For both VASP and WIEN2k GGA+ U calculations, we used U -values ranging from

1.4 to 6.4 eV. A nonzero value of Hund's coupling $J = 0.7 \text{ eV}$ has been considered to account for the anisotropy of the interaction²⁸. Different magnetic configurations were checked: a) a ferromagnetic (FM) order, b) a C-type AFM order for which a $\sqrt{2} \times \sqrt{2}$ cell was used, and c) a G-type AFM order for which a $\sqrt{2} \times \sqrt{2} \times 2$ cell was constructed. Given that a C-type AFM order is more stable for LaNiO_2 at a reasonable U value for this metallic nickelate $\sim 4\text{-}5 \text{ eV}$ ^{29,30} (see Appendix Fig. A1), a C-type AFM order was adopted for the other R112 materials for a systematic comparison. We note that a C-type AFM order is also found to be the groundstate in Ref. 31 using GGA+ U with FLL as the double-counting correction.

In VASP, the wave functions were expanded in the plane-wave basis with a kinetic energy cutoff of 500 eV. The reciprocal space integration was carried out with a $16 \times 16 \times 16$ Γ -centered k -mesh for non-magnetic calculations, and a $12 \times 12 \times 16$ Γ -centered k -mesh for antiferromagnetic calculations. For all WIEN2k calculations, an RK_{max} of 7 was used, as well as a k -mesh of $20 \times 20 \times 23$ for non magnetic calculations and $18 \times 18 \times 30$ for antiferromagnetic calculations. The muffin-tin radii used in WIEN2k for LaNiO_2 are 2.50 \AA for La, 1.99 \AA for Ni and, 1.72 \AA for O.

III. RESULTS

A. Structural properties of RNiO_2

Experimentally reported RNiO_2 ($\text{R} = \text{La, Nd}$) nickelates have a tetragonal structure with P4/mmm space group with $a = b \neq c$ ^{15,16}. The R, Ni and O positions are (0.5, 0.5, 0.5), (0,0,0), and (0.5, 0, 0), respectively. Using this data, we construct the structures for the hypothetical RNiO_2 materials whose lattice parameters were subsequently optimized for different R ions within GGA

in a $\sqrt{2} \times \sqrt{2}$ cell with C-type AFM order. The corresponding lattice constants are shown in Table I and are in agreement with those reported in Ref. 32. Cerium was skipped due to its stable 4+ oxidation state. As expected, the lattice parameters decrease as the size of the rare-earth atom decreases with increasing atomic number. The out-of-plane lattice constant (c) gets reduced by 10% across the lanthanide series from La to Lu, the in-plane lattice constant (a) by $\sim 4\%$. We note that the Ni-O in-plane distance corresponds to $a/2$. The R-O distances are in agreement with the sum of ionic radii for the corresponding R^{3+} ion and O^{2-} in 8-fold coordination³³.

B. Non-magnetic Electronic structure

We first investigate the evolution of the non-magnetic (NM) electronic structure of LaNiO_2 for independent in-plane and out-of-plane lattice constant reductions and then correlate these with the change in R across the lanthanide series. Fig. 1 shows the non-magnetic band structure for LaNiO_2 at the experimental lattice parameters compared with that at 4, and 8% reduction of in-plane (right) and out-of-plane (left) lattice constants (a zoomed-in version of the band structures around the Fermi level is shown in Fig. A2). In all cases, a single $\text{Ni-d}_{x^2-y^2}$ band crosses the Fermi level. In addition, there are La-5d bands that give rise to two electron pockets that self-dope the $\text{Ni-d}_{x^2-y^2}$ band, as determined in previous work on LaNiO_2 and NdNiO_2 ^{30,32,34-37}. The pockets at Γ and A have predominant La- d_{z^2} and La- d_{xy} character, respectively.

Even though upon reducing the lattice parameters there are still bands of $\text{Ni-d}_{x^2-y^2}$ and La- $d_{xy}+d_{z^2}$ character crossing the Fermi level (E_F), important differences arise upon changing the in-plane lattice parameter. In contrast, altering the out-of-plane lattice constant does not give rise to appreciable differences in the bandstructure (see Fig. 1). Specifically, upon reducing the in-plane lattice constant (or Ni-O in-plane distance) the most important modifications in the bandstructure are: 1) The increase in size of the La-d pockets both at A and at Γ . An increase in the size of the R-d pocket at A has been linked to the increase of the hopping between the interstitial and R- d_{xy} orbitals in Ref. 38 when studying trends on different hypothetical d^9 layered nickelates. 2) The increase in the bonding-antibonding splitting of the $\text{Ni-d}_{x^2-y^2}$ and O- $p\sigma$ states, noticeable at the M point (2 eV increase upon an 8% in-plane lattice parameter reduction with respect to the experimental value). 3) The increase in bandwidth of the $\text{d}_{x^2-y^2}$ band crossing the Fermi level (from 3 eV for the experimental lattice constants to 4.6 eV for an 8% reduction of a). These trends are the expected ones: as the in-plane Ni-O distance decreases, the effective $\text{d}_{x^2-y^2}$ nearest neighbor hopping t increases, and so does the bandwidth. The La-d pockets increase to compensate for the overall upward shift of the $\text{Ni-d}_{x^2-y^2}$ band as the lattice parameters are reduced.

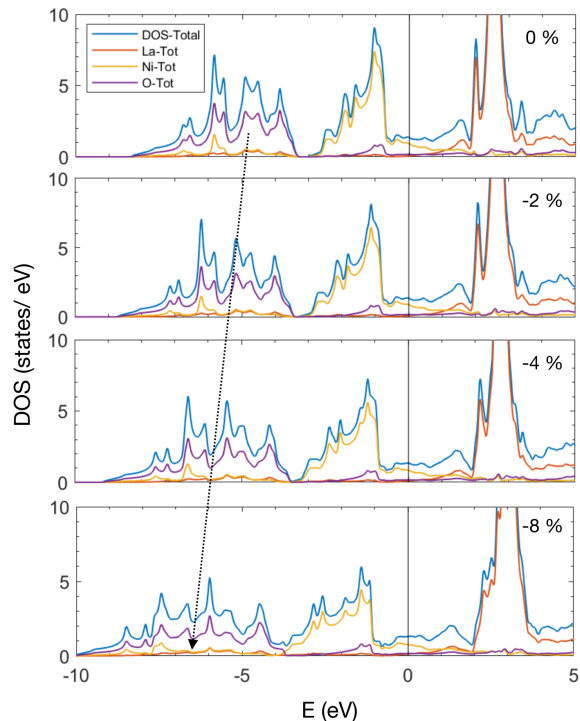


FIG. 2. Total, La-d+f, Ni-d and O-p atom-resolved density of states for GGA non-magnetic calculations in LaNiO_2 for decreasing in-plane lattice parameter with respect to the experimentally reported a value. For each plot, the out-of-plane lattice parameter, c , is held constant.

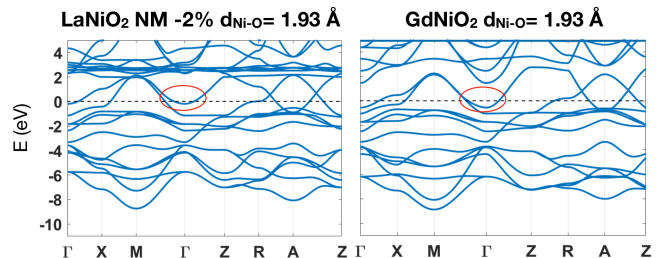


FIG. 3. GGA non-magnetic bandstructure for 1) LaNiO_2 with a 2.4% reduction of the in-plane lattice constant with respect to the experimental value (left), and 2) GdNiO_2 (right). Both systems are compared as they have the same Ni-O in-plane distance. The red oval encloses the R-d electron pocket at Γ .

An important difference between 112 nickelates and cuprates, that has been highlighted before,^{34,35} is the larger charge transfer energy ($\Delta = E_d - E_p$) in the former. The Δ value derived from on-site energies of the Wannier functions for LaNiO_2 is ~ 4.4 eV³⁵ whereas typical cuprate values are ~ 2 eV³⁹. This would put 112 nickelates within the Mott-Hubbard regime in the Zaanen-Sawatzky-Allen classification⁴⁰ in contrast to cuprates, a prototypical example of charge transfer insulator due to the high degree of p-d hybridization⁴¹. Fig. 2 shows the orbital resolved density of states for different in-plane lat-

tice parameter reductions within LaNiO_2 with respect to the experimental value. The most important change in Fig. 2 upon a Ni-O in-plane distance reduction (adding up to effects 1-3 mentioned above) is 4) is the shift of the O-p centroid to lower energies (~ 2 eV shift for an 8% a reduction, 1 eV for a 4% a reduction) while the Ni-d centroid does not significantly move. This last point is very important since it gives rise to a decrease in the degree of p-d hybridization (or an increase in charge transfer energy) as the Ni-O in-plane distance is reduced. This is consistent with Ref. 32 that reports a reduction in p-d hybridization as R changes from La to Lu (i.e. as the lattice parameter is reduced) as inferred from the degree of oxygen admixture in the lower Hubbard band.

Effects 1-4 in the electronic structure derived from a simple in-plane lattice parameter reduction in LaNiO_2 , can be correlated directly to R changes across the lanthanide series by comparing electronic structures that correspond to the same Ni-O in-plane distance. For example, a $\sim 2.4\%$ in-plane lattice constant reduction in LaNiO_2 can be compared directly with the bandstructure of GdNiO_2 as they correspond to the same Ni-O distance of 1.93 Å. Fig. 3 shows the band structures for these two systems. The bandwidth of the $d_{x^2-y^2}$ bands is identical in the two cases (extending from ~ 2 to -1 eV), as is the energy range of the O-p (from ~ -4 to -9 eV) and Ni-d (from ~ 2 to -3.7 eV) states. Also identical is the position of the O-p centroid. The explicit change in R only gives rise to a slightly different size of the R-d pocket at Γ (marked in red). The same reasoning can be extended to the other R ions (see Appendix Figures A3, A4, and A5 for more details).

In essence, all the changes in the electronic structure of RNiO_2 nickelates linked to a change in R (namely the bandwidth, size of the R-d pockets and charge transfer energy), can be mimicked by a simple change of in-plane lattice constant corresponding to the same Ni-O distance. In contrast, a large change in out-of-plane lattice constant has negligible effects in the electronic structure. Hence, we conclude that the relevant control parameter for the electronic structure of 112 nickelates is the Ni-O in-plane distance. A change in R has, per se, negligible effects in the electronic structure, an expected outcome given their chemical similarity. It is simply the Ni-O in-plane distance reduction a change in R gives rise to (as the size of R gets reduced from La to Lu) that has profound effects in the electronic structure. This result contrasts with Ref. 32 in that we find no significant effects that we can ascribe to a specific rare-earth or to the change in out-of-plane lattice constants.

C. Spin-polarized calculations

Strong antiferromagnetic correlations are considered a key ingredient in cuprates. In contrast, there is no experimental evidence for antiferromagnetic order in 112 nickelates to date^{16,18,19}. Recent DMFT calculations in

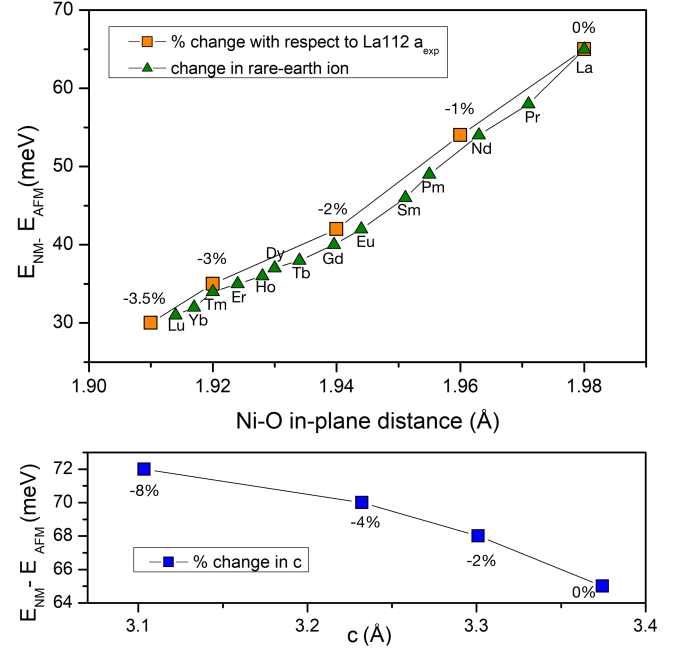


FIG. 4. Energy difference within GGA between a C-type AFM state and a NM state for 112 nickelates as a function of: 1) Ni-O in-plane distance corresponding to changes in R and to a lattice parameter reduction with respect to the experimentally reported a value for LaNiO_2 (top panel) and 2) out-of-plane lattice parameter reduction with respect to the experimentally reported c value for LaNiO_2 (bottom panel).

112 nickelates point to the importance of a multiorbital picture with low-energy relevance of a flat Ni- d_{z^2} band, and the existence of high spin Ni d^8 ⁴²⁻⁴⁵. DFT calculations using C-type AFM order in NdNiO_2 are consistent with this picture in that they also show a flat Ni- d_{z^2} band arising at the Fermi level⁴⁶. This work concludes that this flat band may be related to instabilities that could limit AFM order at low temperature and preclude the AFM phase with the formation of an AFM spin-liquid state that forms the platform for superconductivity⁴⁶. In order to determine the importance and robustness of this flat-band feature in the AFM state for other R ions we analyze, using spin-polarized calculations, different magnetic configurations for RNiO_2 (R= La-Lu) and correlate these trends with in-plane and out-of-plane lattice parameter changes in LaNiO_2 (as done in the previous section for NM calculations).

Both a C-type and a G-type AFM state are more stable than a NM state for LaNiO_2 from first principles. A G-type AFM state is the ground state within GGA (with a small energy difference of 5 meV/Ni with respect to the C-type AFM state, and 70 meV/Ni with respect to the NM state). However, the C-type AFM state becomes more stable than a G-type one within GGA+U for $U \geq 1.4$ eV. This is consistent with the results in Ref. 31 (see Fig. A1 for more details). Attempts to stabilize a FM state give rise to a reduced magnetic moment of $\sim 0.2 \mu_B$

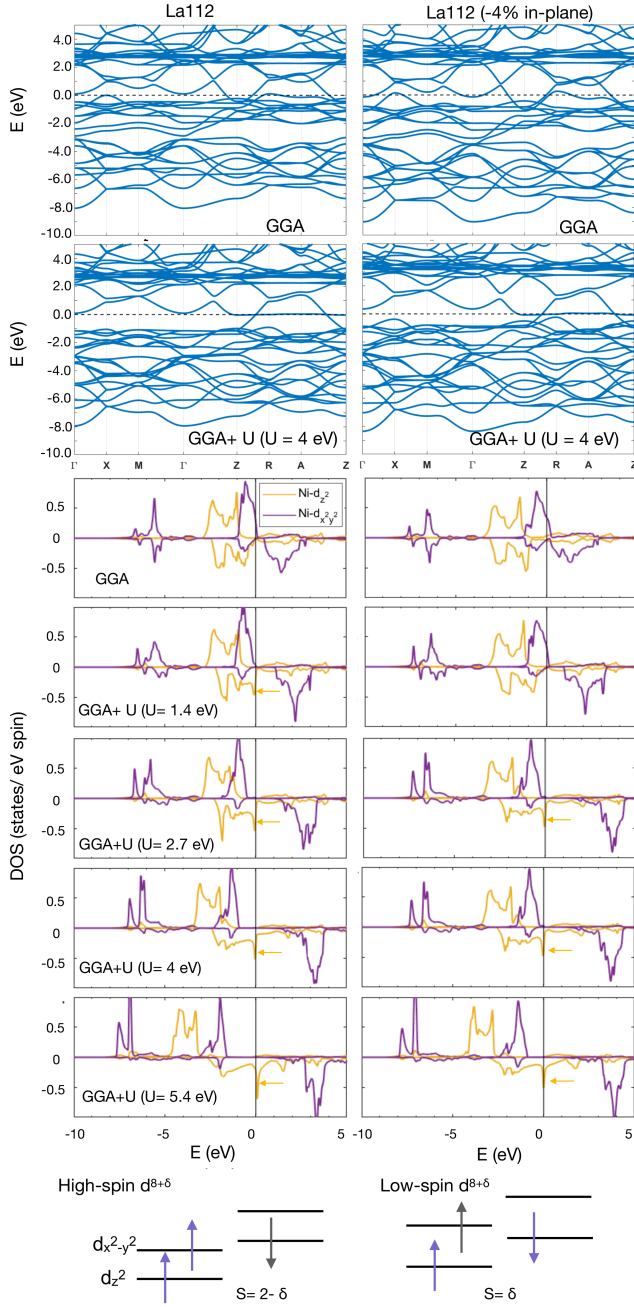


FIG. 5. Top panels: C-type AFM band structure of LaNiO_2 for the experimental lattice parameters (left) and for a 4% a reduction (right) within GGA, and GGA+U (4 eV). Middle panels: Evolution of the $\text{Ni-d}_{x^2-y^2}$ and Ni-d_{z^2} DOS for LaNiO_2 in the AFM state within GGA and GGA+U upon increasing U ($U = 1.4\text{--}5.4$ eV). Note the 1D van Hove singularity pinned at the Fermi level, with pure d_{z^2} character, for $U \geq 1.4$ eV marked by the yellow arrows. Bottom panels: Schematic representation of the energy level diagrams for high-spin $\text{Ni}^{2+\delta}(\text{d}^{8+\delta})$ ion (left) and low-spin (right) in a square-planar environment. The t_{2g} -like levels are fully occupied so we do not show them here. The gray arrow reflects the partial occupation of that particular orbital.

at the GGA level, less stable than any of the AFM states by ~ 0.72 meV/Ni. Note that all these energy differences are small.

As the C-type AFM state is the ground state for a reasonable U value for these metallic nickelates ($U \sim 4\text{--}5$ eV)^{29,30}, this is the AFM order we employ to show magnetic trends in all other RNiO_2 materials to draw a systematic comparison. We note that Ref. 32 describes the evolution of the electronic structure with U in the G-type AFM state instead. G-type AFM order is also the focus of Ref. 47 for NdNiO_2 .

The GGA-energy difference between the C-type AFM state and the NM one for RNiO_2 ($R = \text{La-Lu}$) is shown in Fig. 4 as a function of R and in-plane lattice parameter change. For every R ion and for every lattice parameter used, the ground state of the 112 materials keeps on being AFM. However, as the in-plane lattice parameter/size of R decreases, the energy difference between the AFM and NM state decreases as well (see Fig. 4). Based on these considerations, in contrast to Ref. 32, we anticipate that the tendency towards AFM should be suppressed in R112 as the size of $R/\text{Ni-O}$ in-plane distance is reduced, consistent with the concomitant increase in bandwidth described above. Importantly, the energy difference linked to the in-plane lattice parameter change can be matched almost exactly to that related to a change in R , in agreement with the main conclusion drawn from the NM calculations in the previous section: the change in Ni-O in-plane distance controls the electronic structure of these systems and the R change is not relevant other than for the Ni-O distance change it carries. To further reinforce that the Ni-O in-plane distance is the control parameter in 112 materials, the energy difference between a NM and an AFM state is also shown for an out-of-plane lattice constant reduction. A large 8 % reduction of the out-of-plane lattice constant gives rise to a very small energy difference across the series (~ 7 meV) and does not produce significant changes in the electronic structure.

We now turn to the nature of the AFM state. A simple ionic count for 112 nickelates gives a Ni valence of Ni^{1+} : d^9 , as mentioned above. However, the self-doping effect effectively gives rise to a $\text{d}^{8+\delta}$ ion (with a large δ). In a square planar environment (with a large crystal field splitting between the $\text{d}_{x^2-y^2}$ and d_{z^2} bands) two possible spin states can occur (see Fig. 5). If the crystal field splitting within the e_g states is larger than Hund's rule coupling, a low spin (LS) state develops (with $S = \delta/2$ and a moment $(\delta)\mu_B$ per nickel). If the Hund's rule coupling is larger, a high spin (HS) state would be more stable (with $S = (2-\delta)/2$ and a moment $(2-\delta)\mu_B$ per nickel). The HS and LS states lead to different properties not only in terms of the moments but also in terms of the electronic structure. In particular, for a HS state, Ni-d_{z^2} states are relevant in the vicinity of the Fermi level, in contrast to the more cuprate-like scenario of a LS state, with only a $\text{Ni-d}_{x^2-y^2}$ being relevant. Hence, the careful analysis of HS vs LS states in R112 nickelates is very important.

In this context, it has recently been reported that layered oxychalcogenides $A_2NiO_2Ag_2Se_2$ ($A = Sr, Ba$), with a NiO_2 square lattice and $Ni d^8$, may exhibit HS $S=1$ Ni^{2+48} , or a Ni on-site 'off-diagonal singlet' in which both e_g orbitals are singly occupied but with Kondo-like oppositely spin-directed singlets⁴⁹.

Figure 5 shows the AFM-GGA band structure for $LaNiO_2$ at the experimental lattice parameters and for a 4% in-plane lattice parameter reduction. Both band structures look similar: the derived state is metallic with a $Ni-d_{x^2-y^2}$ band crossing the Fermi level and a La-d pocket around Z. The derived Ni-magnetic moments are consistent with LS-Ni $d^{8+\delta}$ ($\sim 0.7 \mu_B$ for the experimental lattice constants, $\sim 0.6 \mu_B$ for a 4% in-plane lattice parameter reduction). The only differences upon reducing the in-plane lattice parameter are: 1) a slight reduction of the Ni-magnetic moment and 2) an increase in bandwidth, as expected. The same trends are observed for AFM calculations upon a change in R across the lanthanide series (see Figs. A6-A8).

Within GGA+U, the magnetic moments and electronic structure of $LaNiO_2$ at small U value (≤ 1 eV) are very similar to those obtained within GGA, with a $Ni-d_{x^2-y^2}$ and La-d band crossing the Fermi level. At a U value of 1.4 eV, a flat d_{z^2} band emerges at E_F as shown in Fig. 5 that depicts the $Ni-d_{z^2}$ and $Ni-d_{x^2-y^2}$ DOS upon increasing U and shows the corresponding bandstructure at $U=4$ eV. In this bandstructure the flat band can be clearly observed along the Z-R-A-Z direction (for the bandstructures at other U values see Appendix Fig. A9). We find that this feature is robust in DFT for $LaNiO_2$ (and other Rs, see below), in agreement with what Ref. 46 reports for $NdNiO_2$ within DFT, and also in agreement with recent DMFT work⁴²⁻⁴⁵. We note that the La-d states appear well below the Fermi level (see Appendix Fig. A10). As U increases, so does the value of the Ni magnetic moment from the $0.7 \mu_B$ obtained within GGA for the experimental lattice constants, up to $\sim 1.3 \mu_B$ within GGA+U for the highest U value shown of 5.4 eV. This change in the electronic structure is consistent with a LS-to-HS transition with increasing U (even though this behavior had been observed before in DFT calculations^{35,46}, it had never been ascribed to a LS-to-HS $Ni-d^{8+\delta}$ transition).

The metallic character of the AFM state obtained for La_{112} , the LS-to-HS transition upon increasing U, and

the flat d_{z^2} -band feature are robust upon reduction of the in-plane lattice parameter (as shown in Fig. 5) and, more importantly, upon a change in R (see Figs. A6-A9). All in all, this peculiar AFM state with a flat d_{z^2} band pinned at the Fermi level is stable from first-principles calculations for every R and every lattice parameter. Hence, we anticipate the instabilities limiting AFM order at low temperature described in Ref. 46 might be in action in all other parent $RNiO_2$ materials if they can be synthesized.

IV. CONCLUSIONS

Using DFT calculations, we have analyzed the evolution of the electronic structure and magnetic properties of $RNiO_2$ nickelates as R changes across the lanthanide series. By correlating these changes with in-plane and out-of-plane lattice parameter reductions in $LaNiO_2$ (the extreme member of the series), we determine that the electronic and magnetic responses of infinite-layer nickelates are governed by the in-plane Ni-O distance. In contrast, changes in out-of-plane lattice constant have negligible effects. The non-cuprate like properties reported for $La/NdNiO_2$ persist for other rare-earth ions, i. e. involvement of R-bands at the Fermi level and large charge transfer energy. The ground state for $RNiO_2$ materials from first-principles calculations for every R and lattice parameter studied is AFM and metallic, even though the tendency towards AFM is suppressed as the size of R gets reduced from La to Lu. In contrast to cuprates, this AFM state is characterized by multi-orbital character with a flat $Ni-d_{z^2}$ band pinned at the Fermi level (in addition to the naively expected $d_{x^2-y^2}$ states) that enables the formation of high-spin Ni states. It was recently suggested⁴⁶ that for $NdNiO_2$ this flat band can make the system unstable with respect to charge, spin, and lattice orders, limiting AFM order at low temperature. The robustness of this flat d_{z^2} band for every R (and lattice parameter) in $RNiO_2$ nickelates suggests that the same instabilities may arise across the lanthanide series if other members can be synthesized.

V. ACKNOWLEDGMENTS

We acknowledge fruitful discussions with V. Pardo. ASB acknowledges NSF-DMR grant 1904716. We acknowledge the ASU Research Computing Center for HPC resources.

* antia.botana@asu.edu

¹ M. R. Norman, *Reports on Progress in Physics* **79**, 074502 (2016).

² P. Hansmann, X. Yang, A. Toschi, G. Khaliullin, O. K. Andersen, and K. Held, *Phys. Rev. Lett.* **103**, 016401 (2009).

³ J. Chaloupka and G. Khaliullin, *Phys. Rev. Lett.* **100**, 016404 (2008).

⁴ S. Catalano, M. Gibert, J. Fowlie, J. Íñiguez, J.-M. Triscone, and J. Kreisel, *Rep Prog Phys* **81**, 046501 (2018).

⁵ J. Varignon, M. N. Grisolia, J. Íñiguez, A. Barthélémy, and M. Bibes, *npj Quantum Materials* **2**, 21 (2017).

- ⁶ S. Middey, J. Chakhalian, P. Mahadevan, J. Freeland, A. Millis, and D. Sarma, *Annual Review of Materials Research* **46**, 305 (2016).
- ⁷ V. V. Poltavets, K. A. Lokshin, M. Croft, T. K. Mandal, T. Egami, and M. Greenblatt, *Inorg. Chem.* **46**, 10887 (2007).
- ⁸ V. V. Poltavets, K. A. Lokshin, S. Dikmen, M. Croft, T. Egami, and M. Greenblatt, *Journal of the American Chemical Society* **128**, 9050 (2006).
- ⁹ J. Zhang, A. S. Botana, J. W. Freeland, D. Phelan, H. Zheng, V. Pardo, M. R. Norman, and J. F. Mitchell, *Nature Physics* **13**, 864 (2017).
- ¹⁰ A. S. Botana, V. Pardo, and M. R. Norman, *Phys. Rev. Materials* **1**, 021801 (2017).
- ¹¹ D. Li, K. Lee, B. Y. Wang, M. Osada, S. Crossley, H. R. Lee, Y. Cui, Y. Hikita, and H. Y. Hwang, *Nature* **572**, 624 (2019).
- ¹² D. Li, B. Y. Wang, K. Lee, S. P. Harvey, M. Osada, B. H. Goodge, L. F. Kourkoutis, and H. Y. Hwang, *arXiv*, 2003.08506 (2020).
- ¹³ S. Zeng, C. S. Tang, X. Yin, C. Li, Z. Huang, W. L. Junxiong Hu, G. J. Omar, H. Jani, Z. S. Lim, K. Han, D. Wan, P. Yang, A. T. S. Wee, and A. Ariando, *Arxiv*, 2004.11281 (2020).
- ¹⁴ V. I. Anisimov, D. Bukhvalov, and T. M. Rice, *Phys. Rev. B* **59**, 7901 (1999).
- ¹⁵ M. Hayward and M. Rosseinsky, *Solid State Sciences* **5**, 839 (2003), international Conference on Inorganic Materials 2002.
- ¹⁶ M. A. Hayward, M. A. Green, M. J. Rosseinsky, and J. Sloan, *Journal of the American Chemical Society* **121**, 8843 (1999).
- ¹⁷ M. Crespín, P. Levitz, and L. Gatineau, *J. Chem. Soc., Faraday Trans. 2* **79**, 1181 (1983).
- ¹⁸ A. Ikeda, T. Manabe, and M. Naito, *Physica C: Superconductivity* **495**, 134 (2013).
- ¹⁹ A. Ikeda, Y. Krockenberger, H. Irie, M. Naito, and H. Yamamoto, *Applied Physics Express* **9**, 061101 (2016).
- ²⁰ G. Kresse and D. Joubert, *Phys. Rev. B* **59**, 1758 (1999).
- ²¹ G. Kresse and J. Furthmüller, *Phys. Rev. B* **54**, 11169 (1996).
- ²² G. Kresse and J. Furthmüller, *Computational Materials Science* **6**, 15 (1996).
- ²³ M.-Y. Choi, K.-W. Lee, and W. E. Pickett, *Phys. Rev. B* **101**, 020503(R) (2020).
- ²⁴ P. Blaha, K. Schwarz, G. K. H. Madsen, D. Kvasnicka, and J. Luitz, Vienna University of Technology, Austria (2001).
- ²⁵ K. Schwarz and P. Blaha, *Computational Materials Science* **28**, 259 (2003).
- ²⁶ J. P. Perdew, K. Burke, and M. Ernzerhof, *Phys. Rev. Lett.* **77**, 3865 (1996).
- ²⁷ A. I. Liechtenstein, V. I. Anisimov, and J. Zaanen, *Phys. Rev. B* **52**, R5467 (1995).
- ²⁸ E. R. Ylvisaker, W. E. Pickett, and K. Koepnik, *Phys. Rev. B* **79**, 035103 (2009).
- ²⁹ H. Sakakibara, H. Usui, K. Suzuki, T. Kotani, H. Aoki, and K. Kuroki, *arXiv*, 1909.00060 (2019).
- ³⁰ Y. Nomura, M. Hirayama, T. Tadano, Y. Yoshimoto, K. Nakamura, and R. Arita, *Phys. Rev. B* **100**, 205138 (2019).
- ³¹ T. Liu, H. Wu, T. Jia, X. Zhang, Z. Zeng, H. Q. Lin, and X. G. Li, *AIP Advances* **4**, 047132 (2014).
- ³² E. Been, W. Lee, H. Y. Hwang, Y. Cui, J. Zaanen, T. P. Devereaux, B. Moritz, and C. Jia, *arXiv*, 2002.12300 (2020).
- ³³ R. D. Shannon, *Acta Crystallographica Section A* **32**, 751 (1976).
- ³⁴ K.-W. Lee and W. E. Pickett, *Phys. Rev. B* **70**, 165109 (2004).
- ³⁵ A. S. Botana and M. R. Norman, *Phys. Rev. X* **10**, 011024 (2020).
- ³⁶ G.-M. Zhang, Y.-f. Yang, and F.-C. Zhang, *Phys. Rev. B* **101**, 020501(R) (2020).
- ³⁷ P. Jiang, L. Si, Z. Liao, and Z. Zhong, *Phys. Rev. B* **100**, 201106(R) (2019).
- ³⁸ M. Hirayama, T. Tadano, Y. Nomura, and R. Arita, *Phys. Rev. B* **101**, 075107 (2020).
- ³⁹ C. Weber, C. Yee, K. Haule, and G. Kotliar, *EPL (Europhysics Letters)* **100**, 37001 (2012).
- ⁴⁰ J. Zaanen, G. A. Sawatzky, and J. W. Allen, *Phys. Rev. Lett.* **55**, 418 (1985).
- ⁴¹ M. Jiang, M. Berciu, and G. A. Sawatzky, *Phys. Rev. Lett.* **124**, 207004 (2020).
- ⁴² F. Lechermann, *Phys. Rev. B* **101**, 081110(R) (2020).
- ⁴³ F. Lechermann, *arXiv*, 2005.01166 (2020).
- ⁴⁴ F. Petocchi, V. Christiansson, F. Nilsson, F. Aryasetiawan, and P. Werner, *ArXiv*, 2006.00394 (2020).
- ⁴⁵ P. Werner and S. Hoshino, *Physical Review B* **101**, 041104(R) (2020).
- ⁴⁶ M.-Y. Choi, W. E. Pickett, and K.-W. Lee, *Phys. Rev. Research* **2**, 033445 (2020).
- ⁴⁷ Z. Liu, Z. Ren, W. Zhu, Z. Wang, and J. Yang, *npj Quantum Materials* **5**, 31 (2020).
- ⁴⁸ Y. Matsumoto, T. Yamamoto, K. Nakano, H. Takatsu, T. Murakami, K. Hongo, R. Maezono, H. Ogino, D. Song, C. M. Brown, C. Tassel, and H. Kageyama, *Angewandte Chemie International Edition* **58**, 756 (2020).
- ⁴⁹ H.-S. Jin, W. E. Pickett, and K.-W. Lee, *Phys. Rev. Research* **2**, 033197 (2020).

Appendix A: GGA and GGA+U Electronic structure RNiO₂

Figure A1 shows the energy difference between C-type and G-type AFM ordering ($E_C - E_G$) for LaNiO₂ within GGA and GGA+U at different values of U. Within GGA, $E_C - E_G > 0$ so G-type ordering is more stable. However, for $U \geq 2$, the energy difference is negative, thus the C-type AFM order is more stable. In addition, both C- and G-type AFM states are more stable than a NM state for GGA and for GGA+U at all U-values.

Figure A2 depicts the non-magnetic band structures for LaNiO₂ shown in Fig. 1 in a zoomed-in energy range so that the behavior around the Fermi level can be ascertained more easily. The changes to the band structure are readily apparent for a reduction in the in-plane lattice parameter (increase in Ni-d_{x²-y²} bandwidth and size of La-d pockets), whereas a reduction in the out-of-plane lattice parameter produces negligible changes.

Fig. A3 shows the non-magnetic GGA band structure plots of RNiO₂ for twelve different R ions with associated Ni-O distances. Comparatively, Figure A4 shows the non-magnetic GGA band structure plots of LaNiO₂ for different in-plane lattice parameters, ranging from the

experimental one, to an 8% reduction, along with associated Ni-O distances. One can see the similarities between band structures of comparable Ni-O distance and also the same trend of increasing bandwidth as the Ni-O distance is decreased for different R ions (as in Fig. A3) and for decreasing in-plane lattice parameter (as in Fig. A4).

Figure A5 depicts the non-magnetic R-d+f, Ni-d and O-p atom-resolved density of states plots for eight different R ions in R112. One can notice the increase in charge-transfer energy as the size of R decreases with increasing atomic number across the lanthanide series. The same trends are observed in LaNiO_2 for decreasing in-plane lattice parameter, as shown in Fig. 3 in the main text.

Figures A6, A7, and A8 depict the AFM band structure plots for RNiO_2 for twelve R ions withing GGA and GGA+U ($U=4$ eV, $J=0.68$ eV). The bandwidth can be seen to increase for decreasing lattice parameter, and

a flat Ni-d_{z^2} band appears pinned at the Fermi energy along Z-R-A-Z within GGA+U. For each value of U, the Ni magnetic moment decreases as the size of R decreases with increasing atomic number across the lanthanide series.

Figure A9 shows the AFM band structure plots of LaNiO_2 for different in-plane lattice parameters (experimental (0%) , 2%, and 4% reduction) within GGA and GGA+U ($U= 2.7, 4$, and 5.4 eV, $J=0.68$ eV). The same flat Ni-d_{z^2} band appears pinned at the Fermi energy along Z-R-A-Z for non-zero values of U. For each value of U, the Ni magnetic moment decreases with decreasing in-plane lattice parameter.

Figure A10 shows the La-d orbital-resolved density of states for LaNiO_2 for a C-type AFM order at different in-plane lattice parameters (0% and -4% reduction) within GGA and GGA+U ($U= 1.4, 2.7, 4$, and 5.4 eV).

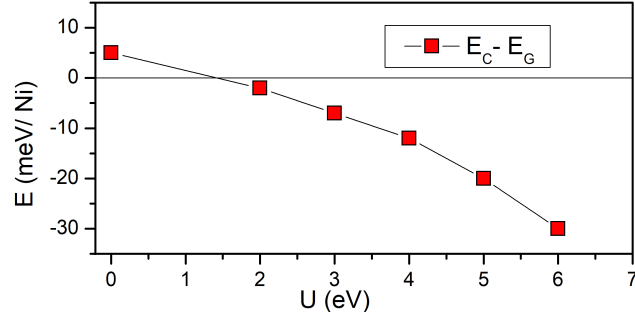


FIG. A1. Energy difference between the two lowest-energy magnetic states (G-type AFM, and C-type AFM) for LaNiO_2 within GGA and GGA+U as a function of U ($U= 2\text{-}6$ eV). Negative indicates C-type is stable, positive indicates G-type is stable.

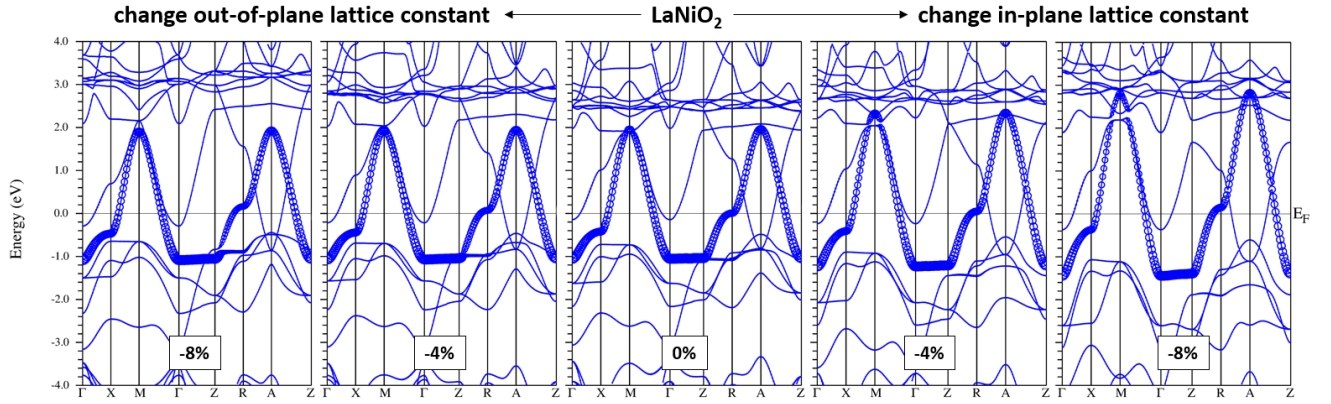


FIG. A2. GGA non-magnetic LaNiO_2 band structure with band character plot ($\text{Ni-d}_{x^2-y^2}$ highlighted) at the experimental lattice constants (0%, central panel), upon reduction of in-plane (right panels) and out-of-plane (left panels) lattice parameters. This is a reproduction of the band structures in Fig. 1 zoomed-in around the Fermi energy.

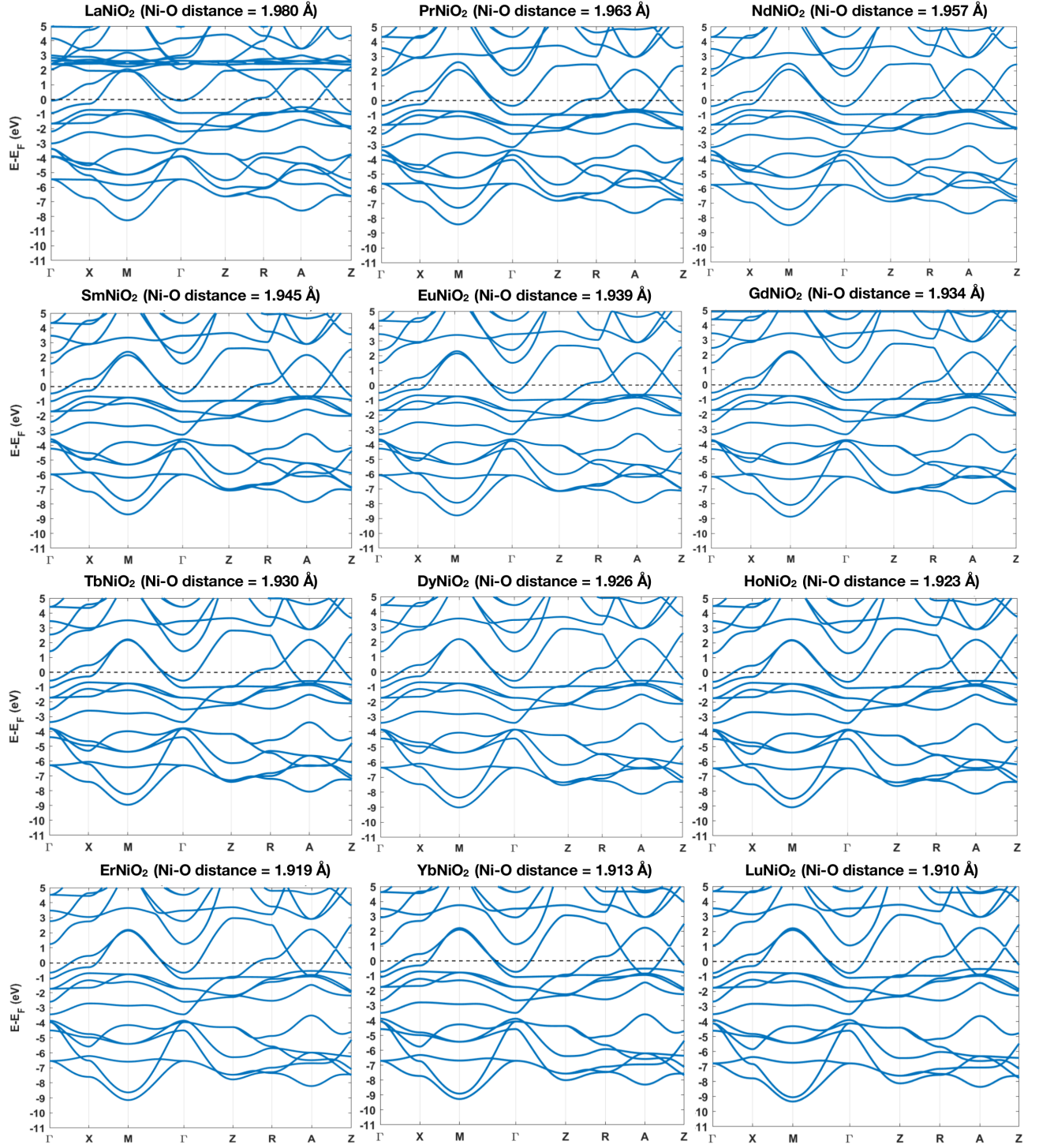


FIG. A3. Non-magnetic GGA band structure plots for RNiO₂ (R= La-Lu).

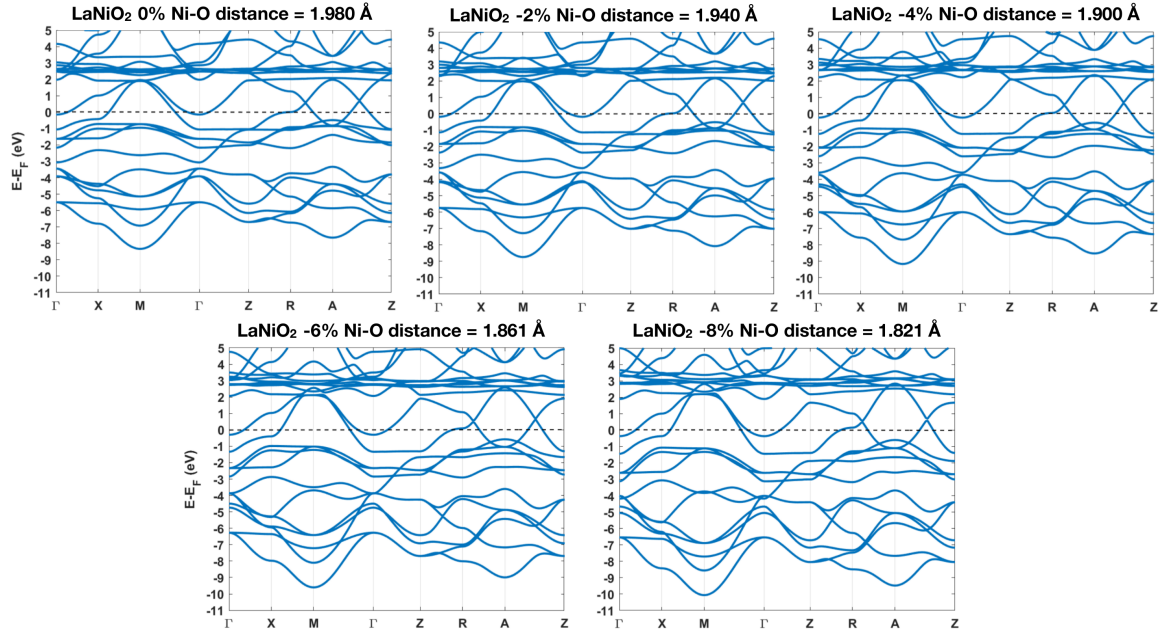


FIG. A4. Non-magnetic GGA band structure plots for LaNiO_2 at different in-plane lattice parameter reductions with respect to the experimental one.

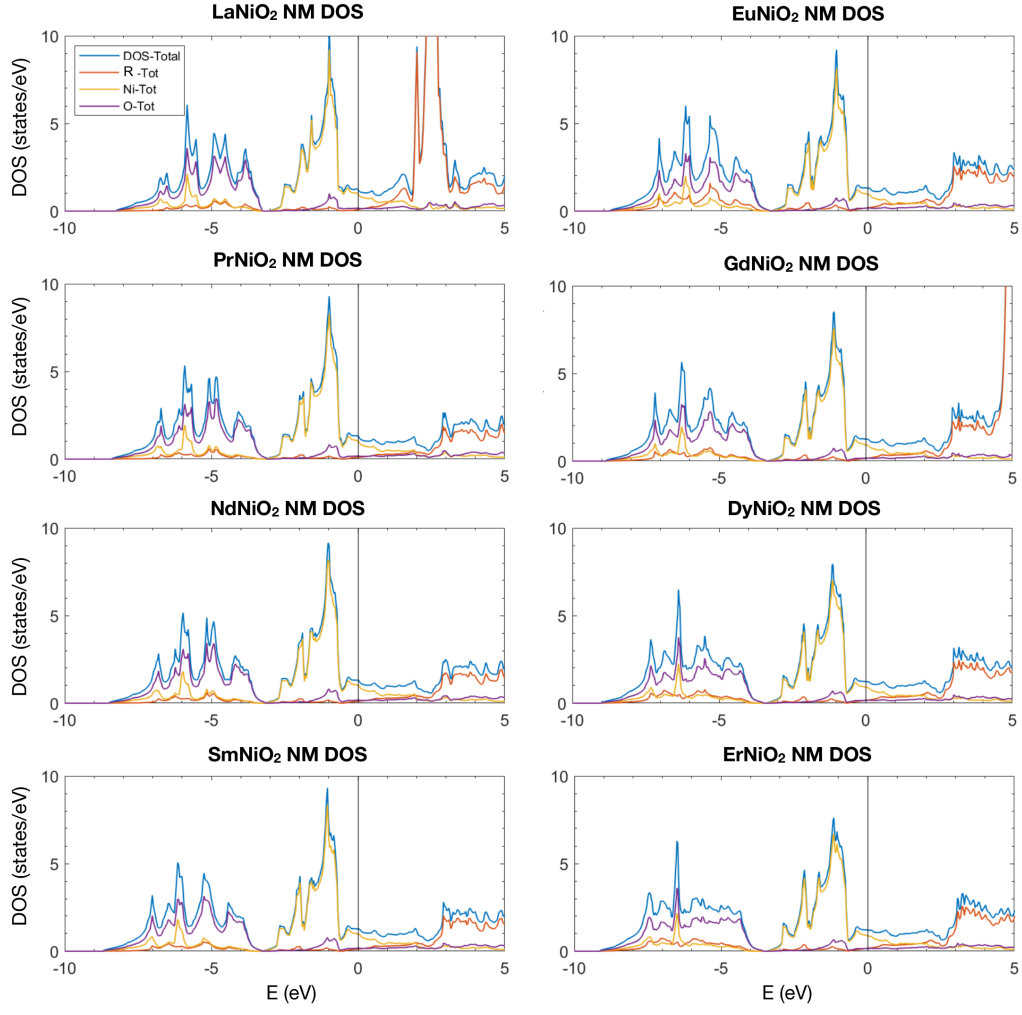


FIG. A5. Total, R-d+f, Ni-d and O-p atom-resolved density of states for different R112.

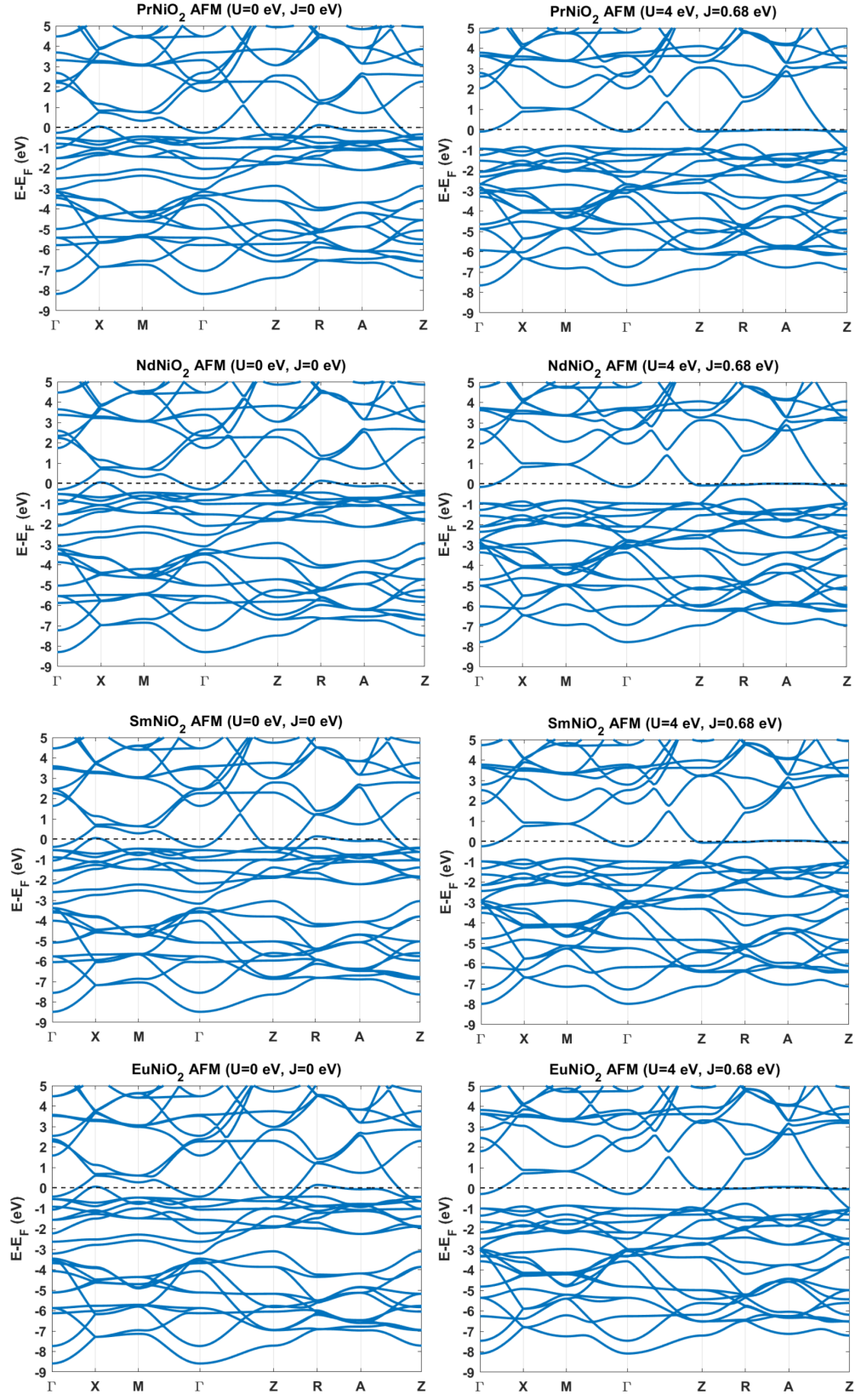


FIG. A6. AFM GGA (left) and GGA+U ($U=4$ eV, right) bandstructure for RNiO_2 . Notice the flat band of Ni- d_{z^2} character pinned at E_F along Z-R-A-Z.

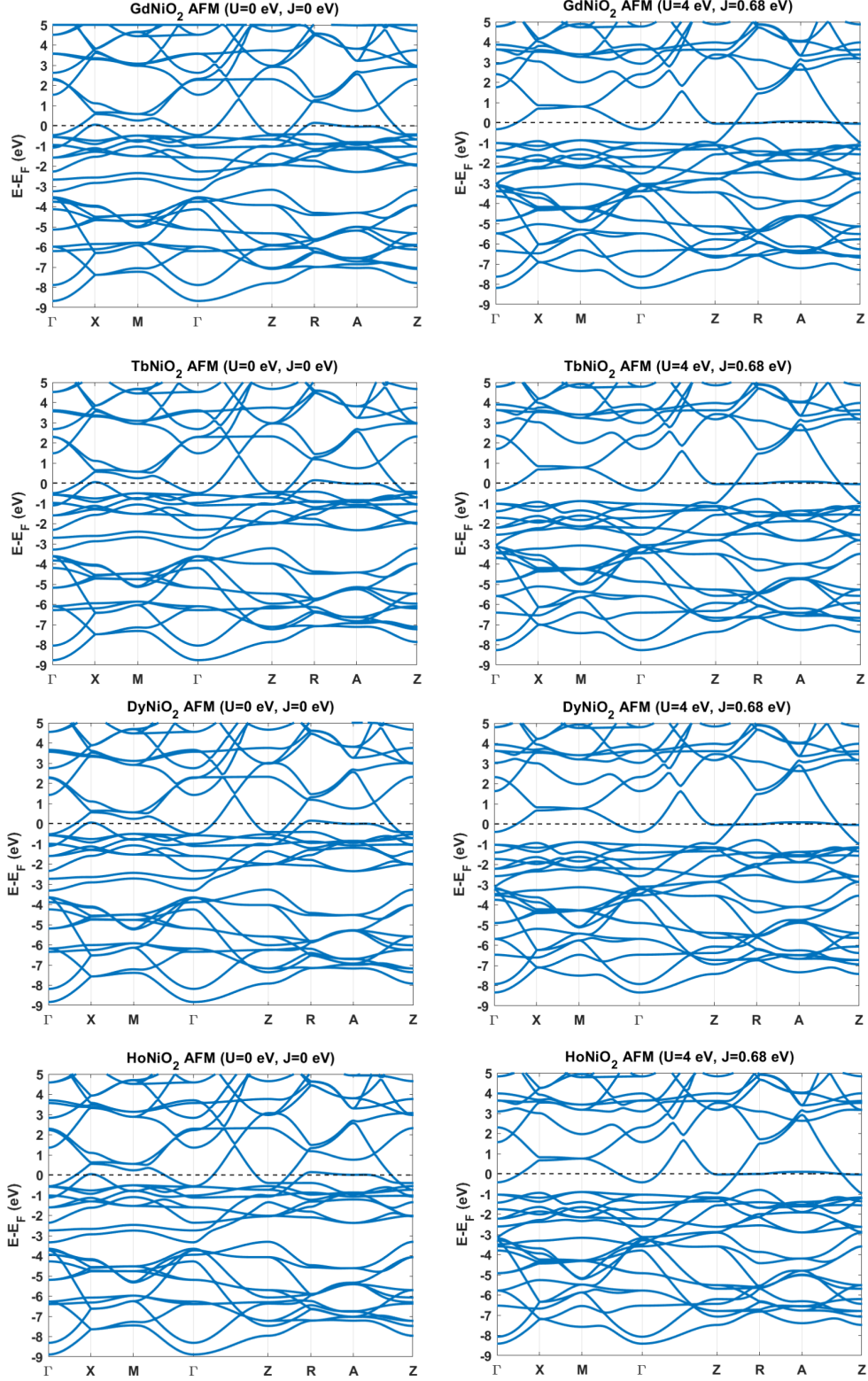


FIG. A7. (continued) AFM GGA (left) and GGA+ U ($U=4$ eV, right) bandstructure for RNiO_2 . Notice the flat band of Ni- d_{z^2} character pinned at E_F along Z-R-A-Z.

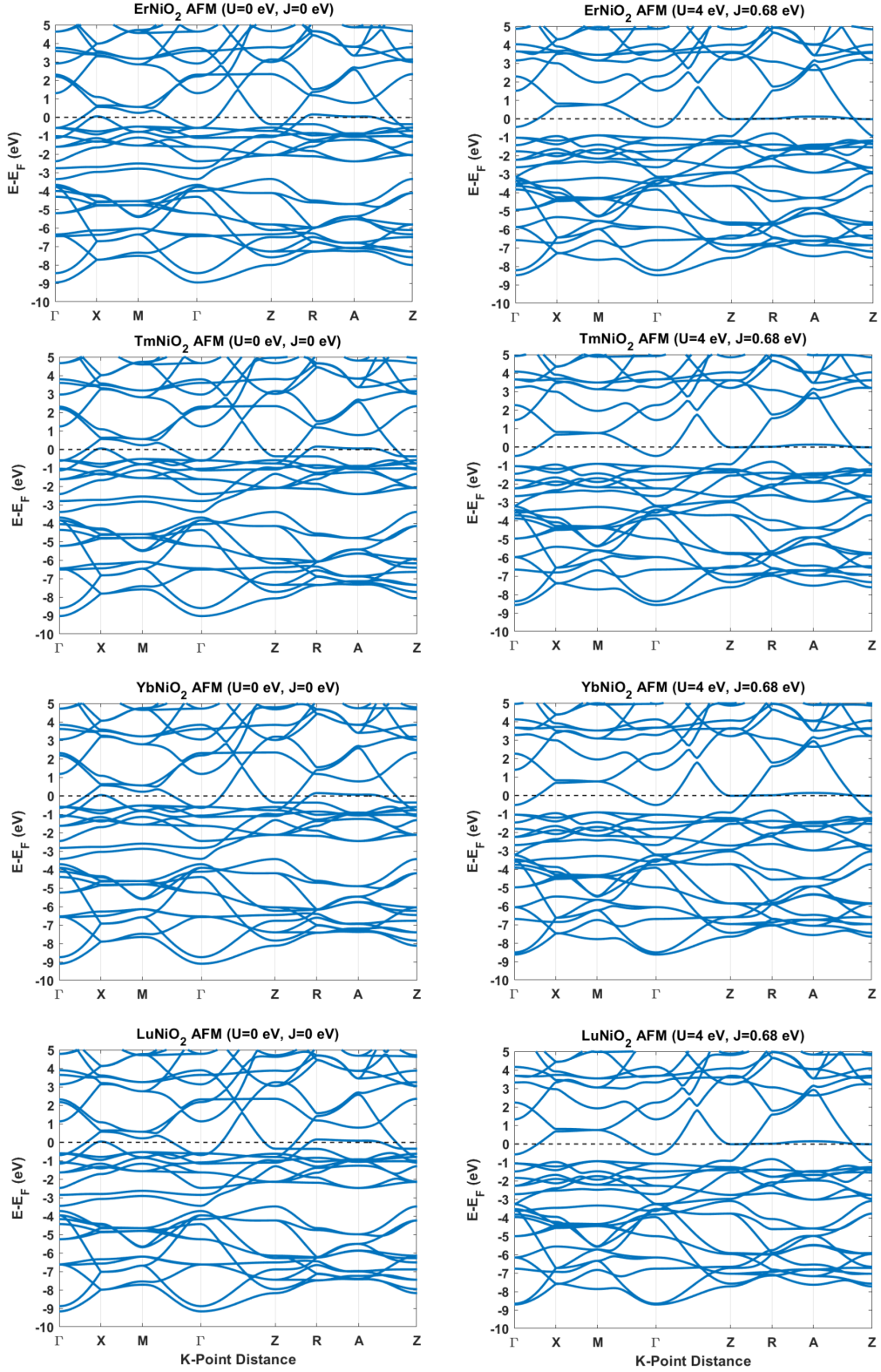


FIG. A8. (continued) AFM GGA (left) and GGA+U ($U = 4$ eV, right) bandstructure for $R\text{NiO}_2$. Notice the flat band of Ni- d_{z^2} character pinned at E_F along Z-R-A-Z.

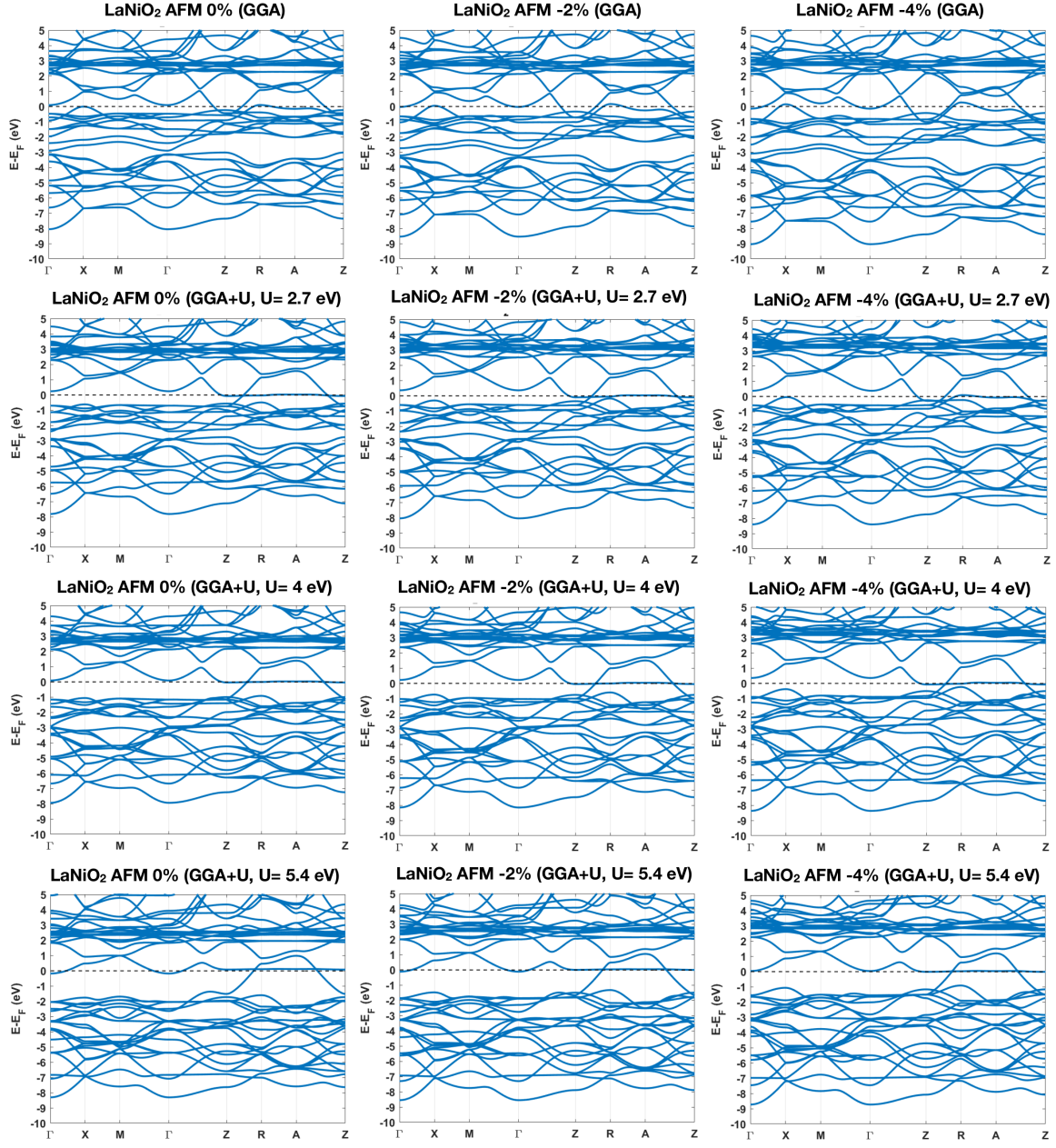


FIG. A9. AFM GGA and GGA+U ($U = 2.7, 4$ and 5.4 eV) band structure plots LaNiO_2 at different in-plane lattice parameters. Notice the flat band of $\text{Ni-d}_{x^2-y^2}$ character pinned at E_F along Z-R-A-Z.

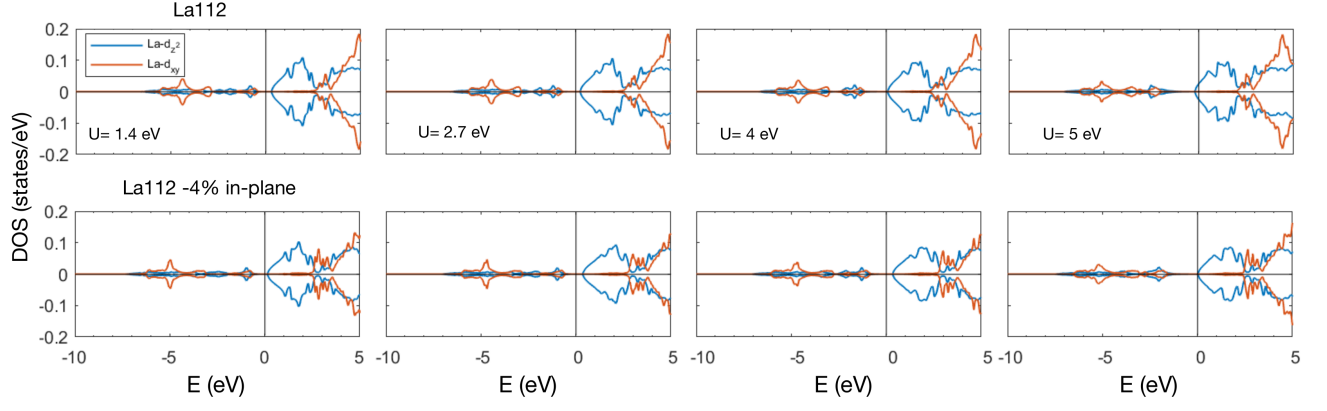


FIG. A10. AFM GGA+U ($U = 1.4$ to 5.4 eV) La-d orbital resolved DOS for LaNiO_2 at different in-plane lattice parameters.